29 April 1994

ELSEVIER

Chemical Physics Letters 221 (1994) 397–406

CHEMICAL PHYSICS LETTERS

Two-dimensional Fourier-transform electron spin resonance in complex fluids

Sanghyuk Lee, Baldev R. Patyal, Sunil Saxena, Richard H. Crepeau, Jack H. Freed

Baker Laboratory of Chemistry, Cornell University, Ithaca, NY 14853-1301, USA

Received 22 November 1993; in final form 2 March 1994

Abstract

Two-dimensional Fourier-transform ESR spectra from a complex fluid characterized by very short free induction decay times are reported. They provide enhanced resolution to dynamic molecular structure compared to conventional cw-ESR spectra which are inhomogeneously broadened by the macroscopic disorder. A general theoretical analysis based on the stochastic Liouville equation permits us to accurately determine the microscopic ordering and motional dynamic rates by non-linear least-squares fitting to experiment.

1. Introduction

ESR has played an important role in the study of the structure and dynamics of complex fluids such as liquid crystals and lipid model membranes due to its high sensitivity and favorable time scale [1]. High-quality studies of such fluids have been performed by cw-ESR using well-aligned samples to yield good spectral resolution to both the microscopic ordering and dynamics [1–4]. For other complex fluids such as viscous liquids, microemulsions, and micellar solutions, as well as membrane vesicles, macroscopically aligned samples are not conveniently available. Instead one must study macroscopically disordered 'dispersion' samples, which may readily be prepared. Nevertheless, ESR has played a useful role in the elucidation of complex fluids despite the limited resolution obtained from such dispersion samples [5–10]. These fluids may typically be characterized as having a microscopic structure but randomness or inhomogeneity on a macroscopic level. Thus, for example, the ESR spectrum from membrane vesicles may be approximated as the superposition of spectra from microscopically well-ordered fragments that are randomly oriented [7,10]. We refer to such cases as MOMD (i.e. microscopically ordered but macroscopically disordered) ESR spectra. It is difficult to discern this inhomogeneous MOMD-broadening effect from the homogeneous line broadening (resulting mainly from the rotational modulation of hyperfine (hf) and g-tensors) and other inhomogeneous broadening (e.g. from proton super-hyperfine (shf) interactions) in cw-ESR spectra, and it results in significantly reduced spectral resolution.

Pulsed ESR methods afford greater sensitivity to spin-relaxation, hence to the molecular dynamics [1,11–13]. Electron spin-echo (ESE) methods have previously been utilized to study viscous fluids in the very slow motional regime [14] as well as oriented lipid membranes [15]. This has included magnetic field-swept 2D-ESE displays of both the homogeneous linewidths [14,15] and the magnetization transfer rates [16] across the spectrum, as well as stepped-field spin-echo ELDOR (electron–electron double

0009-2614/94/$07.00
SSDI 0009-2614(94)00281-T

resonance) in near rigid-limit fluids [17–19].

Modern two-dimensional Fourier-transform (2D-FT) ESR methods have opened up a range of new possibilities [12,13]. These include the study of simple fluids [20] and macroscopically oriented liquid crystals [21] by direct observation of the free induction decay (FID) in two-pulse COSY-ESR and three-pulse 2D-ELDOR, as well as viscous fluids near the rigid limit by collection of the echo decay using two- and three-pulse sequences [22]. These past studies have illustrated the great potential of 2D-FT-ESR to the study of dynamic molecular structure.

Complex fluids are, in general, characterized by short FID decay times, T_2^*, due partly to the inhomogeneities of MOMD, as well as slower motions. In particular, slow motional spectra, as they approach the rigid limit, become even more inhomogeneous with very short T_2^* as previously shown [22]. Thus, in general, complex fluids provide a challenge for these modern ESR techniques.

Because of improvements in instrumental capabilities, viz. shortened spectrometer deadtimes, enhanced signal-to-noise resulting from very rapid signal averaging of successive pulse sequences, and improved data processing and filtering, it is now possible for us to obtain high-quality 2D-FT-ESR spectra from direct observation of the FIDs even with T_2^* as short as 20–30 ns. This has opened up the possibility of applying these powerful methods in the study of complex fluids.

Equally important has been our development of a rigorous theory for the analysis of 2D-FT-ESR spectra. cw-ESR spectra in both the fast and slow motional regimes have for many years been analyzed in the context of a rigorous theory based on the stochastic Liouville equation (SLE) [23–25]. In recent years non-linear least-squares fitting (NLLS) to experiment has been performed utilizing spectral simulations based on the SLE [4,10]. Such methods have proved extremely useful for extracting both dynamic and structural (i.e. ordering) information from reasonably well-resolved cw-ESR spectra. We have now extended the SLE approach to a full and rigorous theory for 2D-FT-ESR that is equivalent in its description of molecular dynamics and ordering to the cw-ESR theory. It is necessarily much more sophisticated in dealing with the spin dynamics as required by these experiments. Improved methods have also enabled us to perform NLLS fitting of sets of 2D-FT-ESR spectra to theory to obtain ordering and dynamic information in an efficient and reliable fashion.

The availability of the second dimension in 2D-FT-ESR simultaneously provides the homogeneous linewidths, the spin-relaxation processes, and details of the sources of the inhomogeneous broadening. In the Letter, we demonstrate how our latest 2D-FT-ESR techniques enable one to elucidate the details of ordering and dynamics in macroscopically disordered complex fluids in a spin-label study of a lipid vesicle system.

2. Experimental

1-palmitoyl-2-oleoyl-*sn*-glycero-phosphatidylcholine (POPC) and the spin probe, 1-palmitoyl-2-(12-doxyl stearoyl) phosphatidylcholine (12PC) were purchased from Avanti Polar Lipids Inc., Birmingham, LA, and were used without further purification.

After a 1 mM solution in chloroform of a mixture of 12PC (1 mol%) with POPC was prepared, it was evaporated to about $\frac{1}{3}$ of its original volume and then transferred to a sample tube (2.5 mm outer diameter, 2.2 mm inner diameter). The remaining chloroform was evaporated by desiccating on the vacuum line for about 12 h. Sufficient water was added to the sample tube to provide a slight excess over that required to saturate the vesicles. The sample was then degassed by several freeze–pump–thaw cycles to a final pressure of about 10^{-4} Torr and sealed.

The 2D-FT-ESR spectrometer is described elsewhere [13,20]. The pulse widths were 5 ns for $\pi/2$ pulses. The 2D-ELDOR sequence is shown in an insert to Fig. 1. The evolution period, t_1, was stepped in 128 steps of 3 ns step size with an initial t_1 value of 50 ns. The FID was collected as a function of t_2 for a total of 256 complex points with a step size of 1 ns (obtained by interleaving [26]) with an initial t_2 value of 67 ns. At each t_1 value, the signal was averaged 600 times for each of the 32 phase cycle steps for 2D-ELDOR. (This is twice the steps reported previously [27].) At a 10 kHz repetition rate, a complete 2D-ELDOR experiment took about 20 min. The experiments were repeated for a series of mixing times, T_m, at several temperatures. The signals were doubly Fourier transformed and utilized for magni-

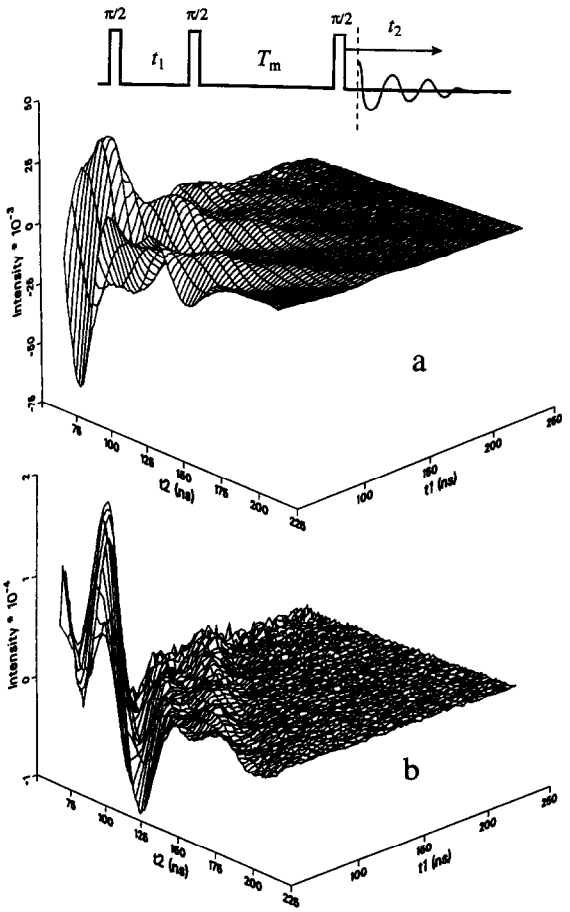

Fig. 1. Time domain 2D-ELDOR spectra for 12PC/POPC vesicles with mixing time of $T_m = 87$ ns at 55°C: (a) S_{c-} signal, (b) S_{c+} signal. Note the difference in scale in (a) and (b). The pulse sequence is shown in insert above.

tude spectra. No filtering or other processing was needed.

3. Theory

In this section, we briefly summarize the strategy for simulating and fitting 2D-ESR spectra. A more complete description will be given elsewhere [28].

The stochastic Liouville equation (SLE) that governs the evolution of the spin density matrix $\rho(\Omega, t)$ can be written as

$$\frac{\partial}{\partial t}\chi(\Omega, t) = -[i\mathscr{H}^{\times}(\Omega) + \Gamma(\Omega)]\chi(\Omega, t)$$
$$\equiv -\mathscr{L}(\Omega)\chi(\Omega, t)\,, \qquad (1)$$

where the modified density matrix $\chi(\Omega, t) = \rho(\Omega, t) - \rho_0(\Omega)$ defines the deviation from the equilibrium density matrix $\rho_0(\Omega)$, $\mathscr{H}^{\times}$ is the commutator superoperator of the spin Hamiltonian, and $\Gamma(\Omega)$ is the time-independent relaxation operator arising from the motional processes [23–25]. Here the Euler angles, Ω, specify the orientation of the molecule. Then the formal solution of Eq. (1) can be written as

$$\chi(\Omega, t+t_0) = \exp(-\mathscr{L}t)\chi(\Omega, t_0)\,. \qquad (2)$$

Thus the evolution of the density matrix is fully described by the eigenmodes of the stochastic Liouville superoperator $\mathscr{L}$, which are obtained by diagonalizing a matrix representation of $\mathscr{L}$.

In the high-field limit, and in the absence of the microwave pulse, the stochastic Liouville matrix is of block-diagonal form in terms of the coherence order of the electron spin p^s [13,24,25,29]. For a spin system with a single electron, the possible values p^s are ± 1 corresponding to the two counter-rotating x–y components of spin magnetization and $p^s = 0$ for the z component of magnetization, and the corresponding stochastic Liouville submatrices may be denoted as $\mathscr{L}_{\pm 1}$ and $\mathscr{L}_0$, respectively. These three matrices may be separately diagonalized by respective complex orthogonal transformations as [13,24,29]

$$O_1^{tr}\mathscr{L}_1 O_1 = \Lambda_1\,, \quad O_0^{tr}\mathscr{L}_0 O_0 = \Lambda_0\,,$$
$$O_{-1}^{tr}\mathscr{L}_{-1} O_{-1} = \Lambda_{-1}\,. \qquad (3)$$

Here the O and Λ matrices are the eigenvectors and the eigenvalues for each subspace with the p^s values specified as a subscript. The detailed expressions for the $\mathscr{L}_i$, the properties of the O_i and the Λ_i, and the matrix diagonalization procedures will be given elsewhere [28].

The effect of the pulse can also be described by Eq. (1). Assuming short and intense pulse we can ignore the contributions of the spin Hamiltonian and the relaxation superoperators during the pulse. The resulting pulse propagator superoperator P shows a characteristic dependence on the phase of the pulse as $\langle p_1^s | P | p_2^s \rangle \propto \exp[-i(p_1^s - p_2^s)\phi]$, which provides the basis for the selection of the coherence pathway

by phase cycling [27,30]. (In this notation $|p_j^s\rangle$ represents the vector in Liouville space for that portion of the density matrix spanning the subspace corresponding to p_j^s.) We abbreviate the effect of the pulse propagator associated with a particular coherence pathway as $P_{(p_1^s \leftarrow p_2^s)}$, where p_1^s and p_2^s are the coherence orders after and before the pulse, respectively.

Any 2D-ESR signal may be expressed in terms of the eigenvalues and eigenvectors of $\mathscr{L}$, and of the pulse propagator. Specifically, the FID signal, whose coherence pathway is $p^s=0\rightarrow -1$ can be written as

$$S^{\mathrm{FID}} \propto \langle \nu_{-1} | O_{-1} \exp(-\Lambda_{-1} t_1) O_{-1}^{\mathrm{tr}} | \nu_{-1} \rangle , \quad (4)$$

where $|\nu_{\pm 1}\rangle = P_{(\pm 1 \leftarrow 0)} \rho_0$, is the density matrix right after the first $\pi/2$ pulse. Similarly, the two-pulse COSY $S_{c\pm}$ signals defined by Gamliel and Freed [27] have coherence pathways $p^s=0\rightarrow \mp 1\rightarrow -1$ and they can be written as

$$S_{c\pm}^{\mathrm{COSY}} \propto \langle \nu_{-1} | O_{-1} \exp(-\Lambda_{-1} t_2) O_{-1}^{\mathrm{tr}} P_{(-1 \leftarrow \mp 1)} \times O_{\mp 1} \exp(-\Lambda_{\mp 1} t_1) O_{\mp 1}^{\mathrm{tr}} | \nu_{\mp 1} \rangle . \quad (5)$$

(The SECSY spectrum [27] is obtained from the COSY S_{c-} signal by replacing t_2 with t_1+t_2.) The ELDOR $S_{c\pm}$ signals with coherence pathway $p^s=0\rightarrow \mp 1\rightarrow 0\rightarrow -1$ are given by

$$S_{c\pm}^{\mathrm{ELDOR}} \propto \langle \nu_{-1} | O_{-1} \exp(-\Lambda_{-1} t_2) O_{-1}^{\mathrm{tr}} P_{(-1 \leftarrow 0)} O_0 \times \exp(-\Lambda_0 T_m) O_0^{\mathrm{tr}} P_{(0 \leftarrow \mp 1)} O_{\mp 1} \times \exp(-\Lambda_{\mp 1} t_1) O_{\mp 1}^{\mathrm{tr}} | \nu_{\mp 1} \rangle . \quad (6)$$

Note that the $S_{c\pm}^{\mathrm{COSY}}$ signals are formally identical to the $S_{c\pm}^{\mathrm{ELDOR}}$ signals for zero mixing time (i.e. $T_m=0$).

The diffusion superoperator $\Gamma(\Omega)$ is described in detail in several places [24,25,31]. For a complex fluid with microscopic structure, we represent the reorientational motion by a rotational diffusion tensor **R**, by the elementary step size, and an orienting potential. In the present study we restricted our analysis to parallel and perpendicular components, $R_\parallel$ and $R_\perp$, and to Brownian (i.e. infinitesimal) jumps. The orienting potential $U(\Omega)$ refers to the molecular orientation relative to its preferred alignment (i.e. the local director). It is expanded in terms of the generalized spherical harmonics [25,31]. We used the restricted sum,

$$U(\Omega) = -k_B T \sum_{L=2,4} [\epsilon_{L0} \mathscr{D}_{00}^L(\Omega) + \epsilon_{L2}(\mathscr{D}_{02}^L(\Omega) + \mathscr{D}_{0-2}^L(\Omega))] , \quad (7)$$

where Ω represents the Euler angles describing the orientation of the principal axes of the ordering tensor (taken to be coincident with those of the diffusion tensor [25,31]) with respect to the director axis. The order parameter $S=\langle D_{00}^2(\Omega)\rangle$ is a measure of the extent of the ordering along the local director.

Another relevant set of Euler angles is Φ representing the tilt of the principal axes for the magnetic tensor relative to the principal axes of the diffusion tensor. For simplicity we let $\Phi=(0, \phi, 0)$.

The ESR spectra from macroscopically disordered fluids can be treated by the MOMD model when there is microscopic ordering. The MOMD spectra are obtained as the superposition of spectra from each microscopically ordered domain, with its local director axis randomly distributed on the unit sphere, i.e.

$$S_{c\pm}^{\mathrm{MOMD}} = \int S_{c\pm} \sin \Psi \, \mathrm{d}\Psi , \quad (8)$$

where Ψ is the angle of the tilt of the local director from the magnetic field direction.

The inhomogeneous broadening arising from the proton shfs can be approximated by a Gaussian distribution, which modifies the unbroadened signal according to [27–30,32]

$$S_{c\pm}^{\mathrm{GIB}} = S_{c\pm} \exp[-2\pi^2 \Delta^2 (t_1 \pm t_2)^2] , \quad (9)$$

where Δ is the width of the distribution in frequency units.

The ability to selectively choose the coherence pathway is a particular advantage of 2D spectroscopy. Suitable linear combinations of the dual quadrature signal results in the $S_{c\pm}$ signals [27]. The principal difference in the two signals is a cancellation of inhomogeneous broadening in the S_{c-} signal. The two eigenvalue sets Λ_1 and Λ_{-1} involved during t_1 and t_2 in the S_{c-} signal (cf. Eqs. (5) and (6)) are complex conjugates of each other when the nuclear Zeeman term is neglected (i.e. $\Lambda_{-1}=\Lambda_1^*$ and also $O_{-1}=O_1^*$) [24,29,32]. This implies the electron spins rotate with opposite sense during t_1 and t_2, leading to the formation of an echo at $t_1=t_2$ where the effect of the inhomogeneous broadening is canceled. (In the presence

of the nuclear Zeeman term, nuclear modulation may be observed in the 2D signal [26,27].)

4. Results and discussion

4.1. Inhomogeneous broadening and MOMD

In the absence of significant inhomogeneous broadening the S_{c+} and S_{c-} signals are equivalent [13,20]. However the ESR spectra for spin-bearing molecules in complex fluids typically exhibit considerable inhomogeneity. First of all the molecular rotational motion is often in the slow motional regime. Secondly, the MOMD effect leads to inhomogeneity. Finally, proton shfs is present. The inhomogeneous broadening causes the S_{c+} and S_{c-} signals to be different, since the S_{c-} signal has the echo-like refocusing property whereas the S_{c+} signal does not. As rotational motion slows down further and/or the microscopic ordering increases, the inhomogeneous broadening becomes much larger than the homogeneous linewidth. The S_{c+} signal decays below the noise level within the spectrometer deadtime and *only* the S_{c-} signal may be collected. When the decay is rapid enough the FID signal will be lost even for S_{c-} in a short time, and only the echo centered about $t_1 = t_2$ will be observed. This is usually the case near the rigid limit.

In our study of 12PC/POPC over the temperature range from 50 to 80°C, rotational rates are already into the slow motional regime, and the near-end-chain label exhibits a small amount of ordering. Thus the S_{c+} and S_{c-} signals are appreciably different, but the S_{c+} signal can still be observed. In Fig. 1 we show typical 2D-ELDOR S_{c+} and S_{c-} FID signals in the time domain. The cancellation of the inhomogeneous broadening along the $t_1 = t_2$ axis is clearly shown in the S_{c-} signal as indicated by the longer persistence of the signal along this axis. The S_{c+} signal does not show any refocusing and decays monotonically. The S_{c+} signal is much weaker than the S_{c-} signal, since a significant portion of the former is lost due the T_2^* decay during the spectrometer deadtimes in t_1 and t_2.

In Fig. 2 we show a set of 2D-ELDOR spectra, both S_{c+} and S_{c-} for different mixing times T_m, obtained at 70°C. The diagonal peaks (i.e. the auto-peaks) in the S_{c-} signal are seen to be sharper than the corresponding auto-peaks in the S_{c+} signal due to suppression of the inhomogeneous broadening in the former. The cross-peaks in the S_{c-} signal have lower height relative to their auto-peaks (due to their relatively larger widths) than is the case for the S_{c+} signal. This is because the S_{c-} cross-peaks have less suppression of inhomogeneous broadening than the auto-peaks (as explained below), whereas neither auto- nor cross-peaks in the S_{c+} signal have any suppression of inhomogeneous broadening.

The inhomogeneous broadening due to the MOMD effect is of particular interest. The local director tilt angle, Ψ is different for each local domain. The local g-values and hf splittings vary with Ψ resulting in a distribution of resonance frequencies [7,10]. Since the weighting of each orientation is proportional to $\sin\Psi$ (cf. Eq. (8)), components with $\Psi \approx 90°$ are more important than components with $\Psi \approx 0°$ in the overall superposition, and this leads to an *asymmetry* of the peaks. The MOMD features become more prominent as the ordering increases, emphasizing the differences between each local domain, but as the rotational rate decreases, slow motional effects can also cause related asymmetric inhomogeneities in cw-ESR.

Unlike simple Gaussian inhomogeneous broadening, the broadening due to MOMD is different for each hf line. For an ^{14}N nitroxide spin label, the outer peaks are affected by both the g- and hf-tensors, whereas the resonance frequency of the central peak is determined only by the g-tensor. At 9 GHz ESR frequency the hf splitting shows more orientational variation. Therefore the two outer peaks are spread over a wide range, whereas the central peak remains fairly sharp. The combined effects of MOMD and of the homogeneous widths do lead to the $m_I = -1$ line being much broader than the other two as is well known [10,21]. Thus, given the finite spectrometer deadtime, only the $m_I = 0$ and $m_I = +1$ auto-peaks have substantial amplitudes. The cross-peak pattern in a 2D-ELDOR experiment is also different from that of simple Gaussian inhomogeneous broadening. The cross-peaks develop as a result of modulation of the hf tensor by the rotational motions, which induces nuclear spin flips [12,13,21]. (An additional cause of cross-peak development is Heisenberg spin exchange, but we found it to be unimportant for the experiments reported here.) These cross-peaks develop for each local domain with its specific director tilt angle. Therefore the cross-peak shape reflects the

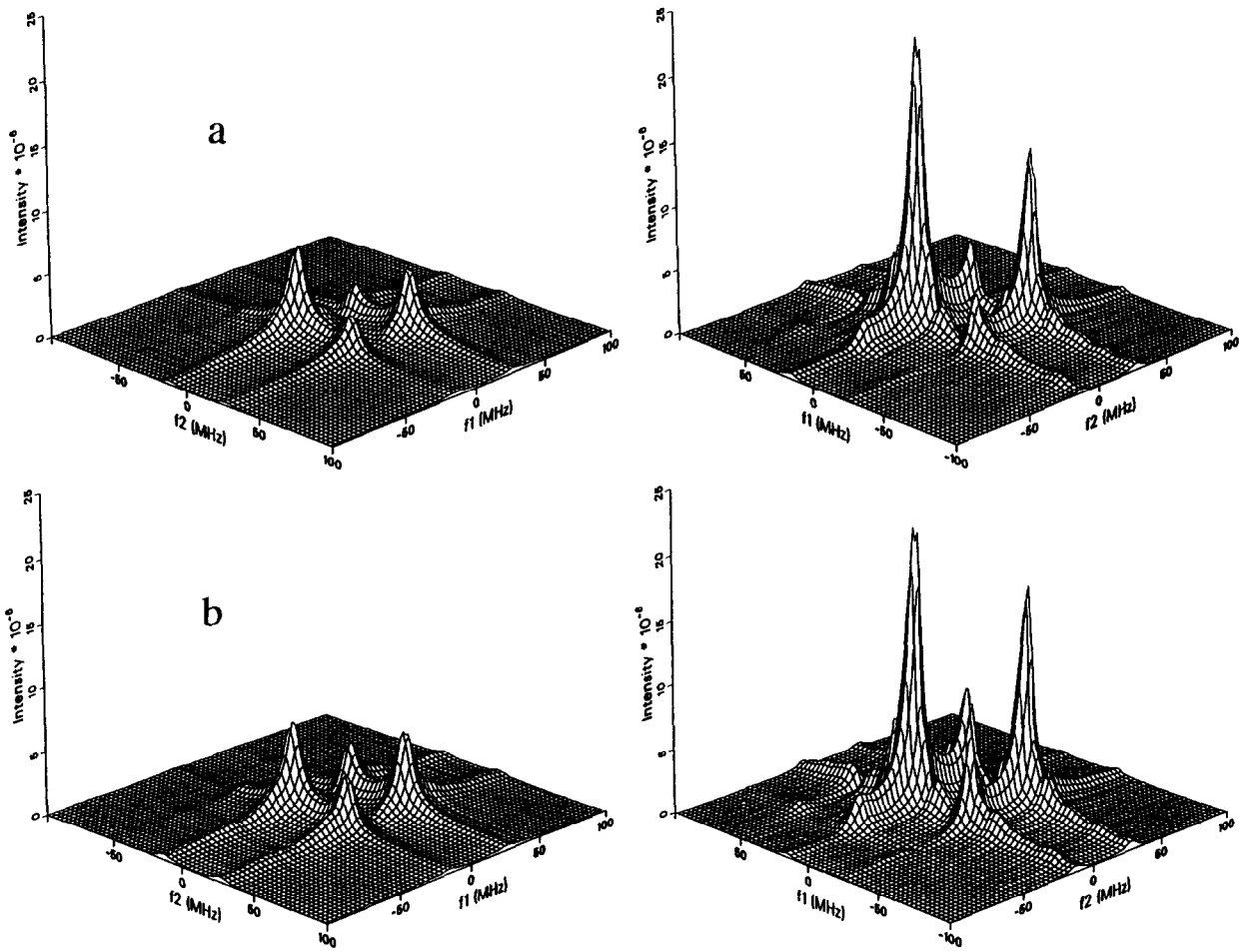

Fig. 2. The experimental 2D-ELDOR spectra as a function of mixing time at 70°C. Both the S_{c+} signal (left) and the S_{c-} signal (right) are shown to the same scale for each temperature. (a) $T_m = 87$ ns, (b) $T_m = 150$ ns, (c) $T_m = 300$ ns, (d) $T_m = 400$ ns.

weighting and the resonance frequencies for each tilt angle as well as the orientation-dependent nuclear spin flips for slow motions, and this leads to a skewed asymmetric ellipsoidal shape. Note, in particular, that the echo-like cancellation for each cross-peak in the S_{c-} signal is incomplete because the MOMD broadening is different during the t_1 and t_2 evolution and detection periods; i.e. cross-peaks arise because spins belong to different hf lines during these periods. This allows further discrimination of the MOMD contribution. The extra broadening of the cross-peaks relative to the auto-peaks in the S_{c-} signal was noted above.

The asymmetries associated with the MOMD model only have a small effect on the 2D-ELDOR in 12PC/POPC spectra from vesicle samples because of the low ordering. Other spin labels can show more prominent effects [33]. The main point is that the shapes of the 2D-ELDOR auto- and cross-peaks are sensitive indicators of the degree of microscopic ordering.

4.2. Analysis of spectra

Considering the complexities involved in the spectra, the best method of analyzing the experimental spectra is by NLLS fitting. The simulation program is coupled with a NLLS fitting program using an improved Levenberg–Marquardt algorithm [28]. It is important to note that we *simultaneously* fit *multiple* 2D spectra (both S_{c+} and S_{c-} spectra for 2D-ELDOR experiments with a series of mixing times) to

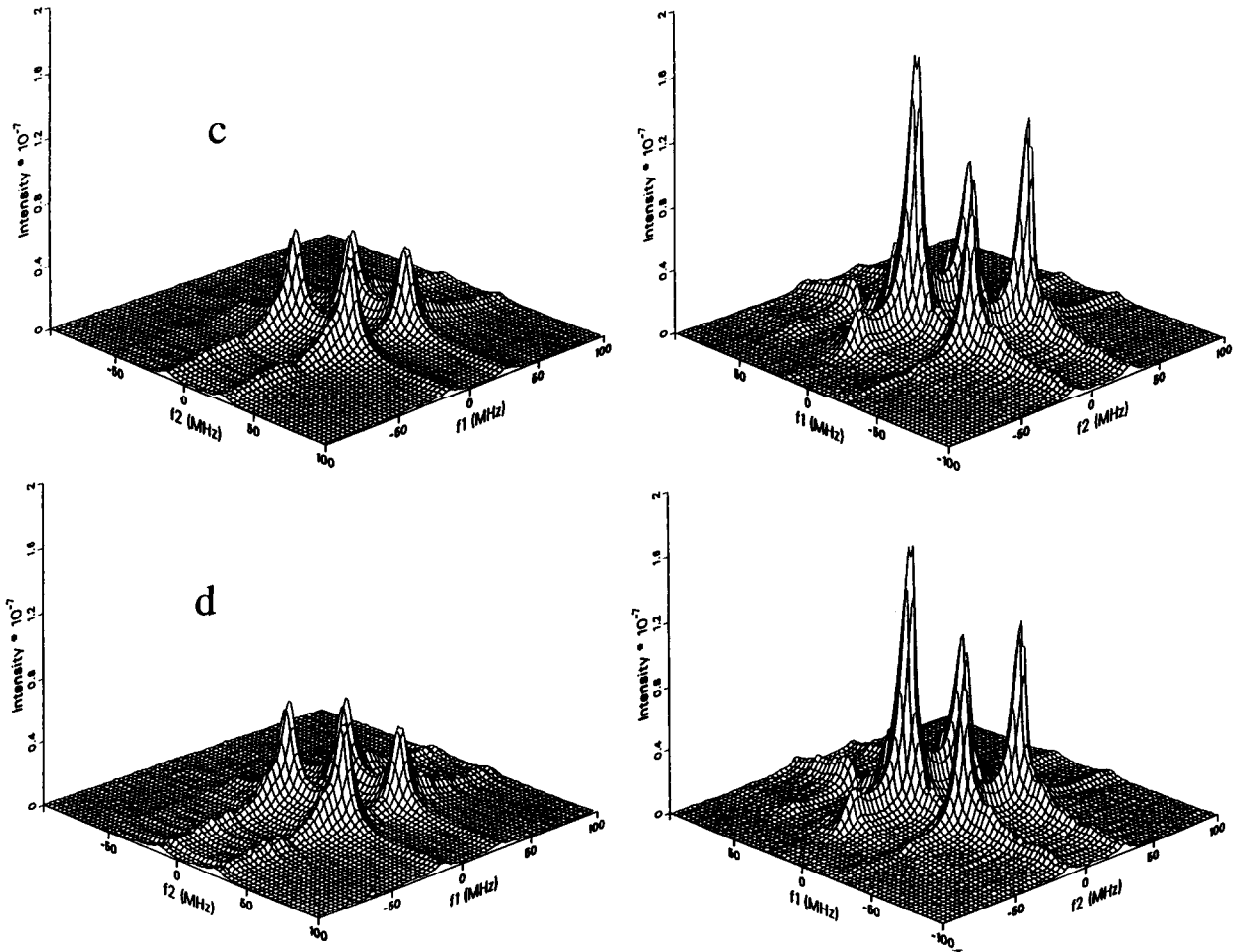

Fig. 2. Continued.

obtain the optimum parameters. This approach is very efficient since all those 2D spectra at each temperature can be simulated using the same eigenvalues and eigenvectors (cf. Eqs. (5) and (6)). This also provides additional accuracy compared to a cw-ESR simulation where only one spectrum is available.

The g- and hf-tensors were obtained from the cw-ESR spectra in the rigid limit, and are $g_x=2.0092$, $g_y=2.0059$, $g_z=2.0021$ and $a_x=a_y=4.9$ G, $a_z=34.2$ G. MOMD spectra were simulated using 15 values of Ψ, which proved to be sufficient. The minimum basis set necessary to represent the stochastic Liouville matrices was obtained according to a pruning scheme analogous to the minimum truncation scheme in cw spectral simulation [24,25]. The dimensions of Λ_1 and Λ_0 were 75 and 132 at 50°C. All the experimentally measured parameters such as magnetic field, spectrometer deadtimes and mixing times, were used in the simulation.

Initial NLLS simulation showed that only $R_\perp$, $R_\parallel$, ϵ_{20}, ϵ_{22}, ϕ, and Δ were significant. The fits were most sensitive to $R_\perp$, ϵ_{20}, ϕ, and Δ and less so to $R_\parallel$ and ϵ_{22}, and we found that $\phi \approx 34°$ and $N \equiv R_\parallel/R_\perp \approx 32$ for all the temperatures. After mixing ϕ and N, the optimum values of the other parameters for the five temperatures are summarized in Table 1. In Fig. 3 we show the NLLS fits to the 70°C results of Fig. 2. One observes that the agreement between experiment and simulation is very good. The fits at the other temperatures are of comparable quality.

The rotational diffusion rate $R_\perp$ decreases with temperature as expected and yields a typical activa-

Table 1
Optimum motional and ordering parameters for the 12PC/POPC system at several temperatures obtained by NLLS fitting [a]

T (°C)	$R_\perp \times 10^{-7}$ (s^{-1})	$R_\parallel \times 10^{-9}$ (s^{-1})	A_G (G)	ϵ_{20}	ϵ_{22}	S
80	8.70	2.75	0.34	0.96	−0.40	0.203
70	6.07	1.92	0.37	0.97	−0.37	0.205
60	4.88	1.54	0.40	0.98	−0.44	0.204
55	4.55	1.44	0.41	0.98	−0.41	0.205
50	4.14	1.31	0.40	1.01	−0.49	0.210

[a] $N \equiv R_\parallel / R_\perp = 32$; $\phi = 34°$.

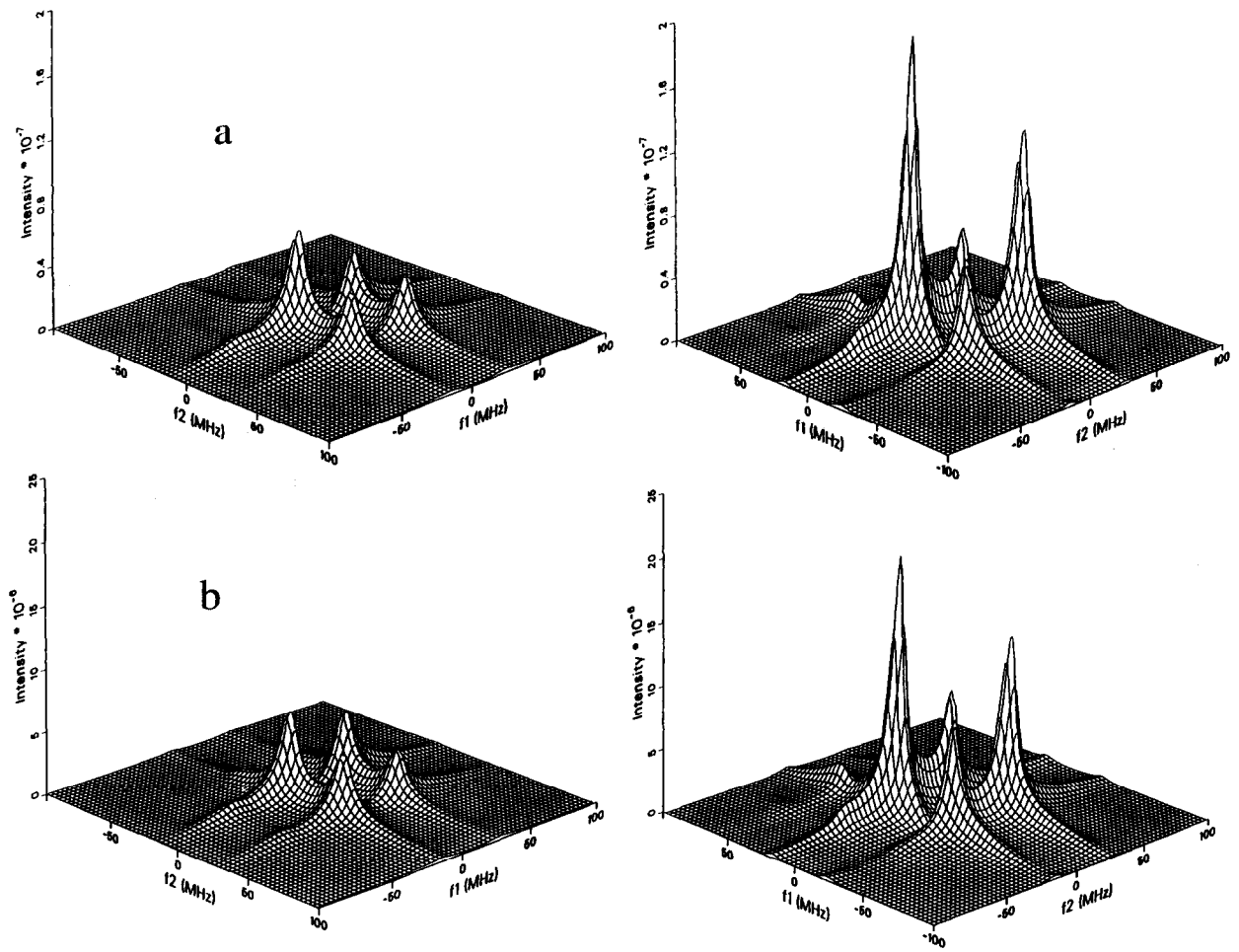

Fig. 3. The simulated 2D-ELDOR spectra corresponding to Fig. 2. The parameters in Table 1 were used. (a) $T_m = 87$ ns, (b) $T_m = 150$ ns, (c) $T_m = 300$ ns, (d) $T_m = 400$ ns.

tion energy of 5.5 kcal mol^{-1} [4]. The order parameter S remains nearly constant with temperature over this range. It is a little larger than the values obtained from a study of aligned 16PC/POPC samples by cw-ESR [4] as expected, since the position of the nitroxide moiety in 16PC is closer to the end of the lipid chain. The value of tilt angle of the nitroxide magnetic tensor relative to the hydrocarbon chain diffu-

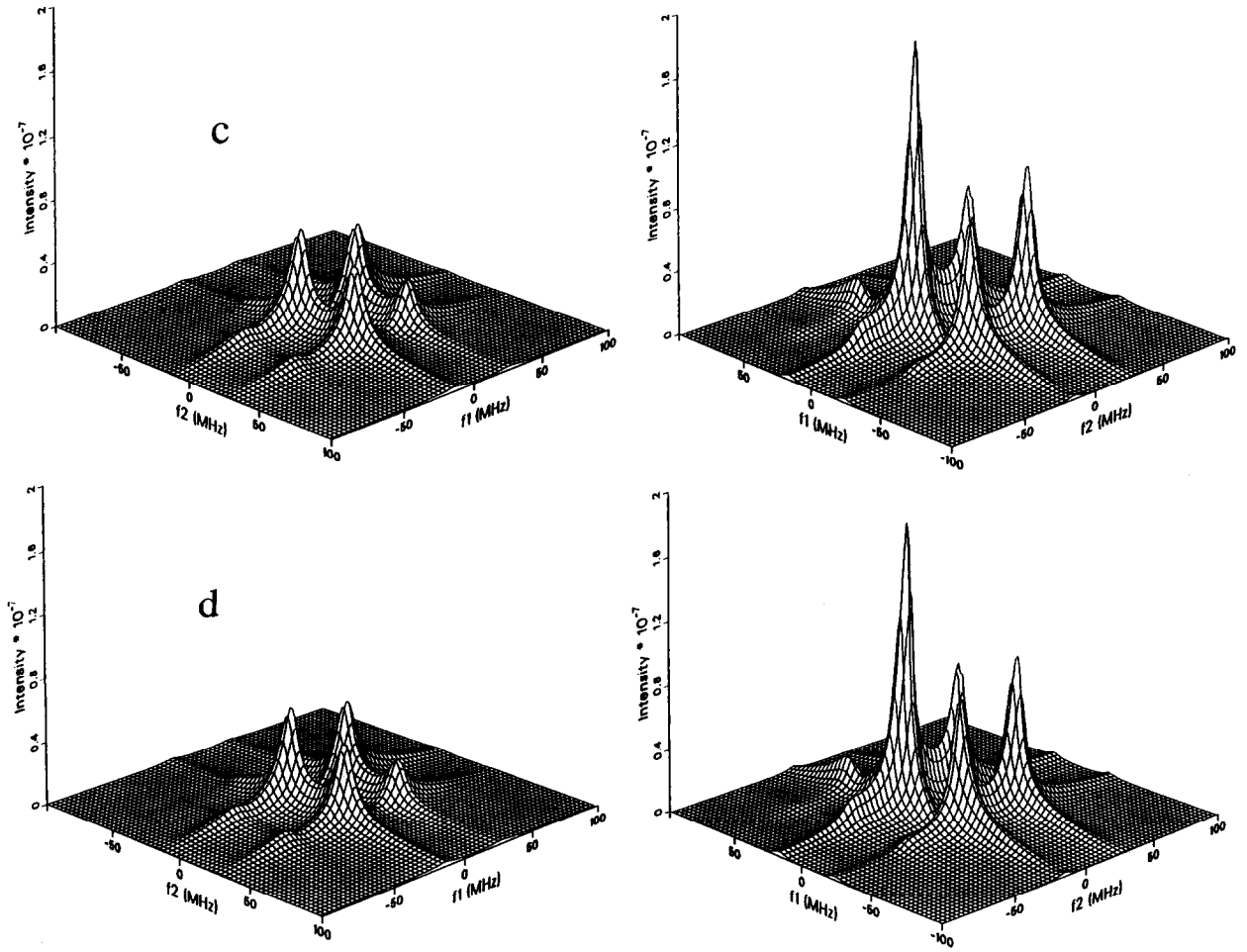

Fig. 3. Continued

sion axis of $\phi = 34°$ corresponds to values found for 10PC and 5PC in a cw-ESR study of dispersions [10], which however could not resolve out both ordering and diffusion parameters.

Although we collected FIDs in our 2D-ELDOR experiments, the S_{c-} signal can still be used to extract the homogeneous widths, because of the cancellation of the inhomogeneous broadening along $t_1 = t_2$ for the auto-peaks. The S_{c-} data with $t_2 > t_1$ are subjected to the axis transformation $t_2 \rightarrow t_1 + t_2$ (i.e. the same transformation used to obtain a SECSY spectrum from a COSY spectrum (cf. Eq. (5)). A subsequent double FT yields the homogeneous lineshapes along f_1. We have performed this transformation and obtained the *apparent* homogeneous linewidths across the spectrum as a function of mixing time, T_m. True homogeneous widths must be independent of T_m. However, as shown in Table 2 for 80°C, these widths (from a linear-predictive analysis [13]) are observed to increase with T_m. We find this extra broadening is reduced as the temperature decreases.

An analogous effect was reported in a 2D-ELDOR single crystal study [26]. We suspect this is due, in the present case, to a slow change in orientation of the local director due either to director fluctuations or to the translation of the 12PC in the vesicle. These are well-known relaxation processes in NMR [34], but are too slow in the ESR time domain [1–3] to be

Table 2
Variation of apparent inverse linewidths (i.e. T_2) with mixing time for each hf auto-peak at 80°C

Mixing time (ns)	T_2 (ns)		
	$m_I=-1$	$m_I=0$	$m_I=+1$
87	55	91	90
150	52	84	87
250	49	81	83
450	47	71	78
750	44	67	71

significant for cw-ESR. Our observation could imply that 2D-ELDOR allows for their direct observation in real time.

In conclusion, we have shown how 2D-ELDOR enables the accurate determination of ordering and dynamics in a complex fluid, and the high degree of spectral resolution enables even subtle effects to be distinguished.

Acknowledgement

This work was supported by NSF Grants CHE9313167 and DMR9210638 and NIH Grants GM25862 and RR07126. Computations were performed at the Cornell National Supercomputer Facility.

References

[1] J.H. Freed, in: Rotational dynamics of small and macromolecules in liquids, eds. T. Dorfmuller and R. Pecora (Springer, Berlin, 1987).
[2] A. Nayeem and J.H. Freed, J. Phys. Chem. 93 (1989) 6539.
[3] A. Nayeem, S.B. Rananavare, V.S.S. Sastry and J.H. Freed, J. Chem. Phys. 96 (1992) 3912.
[4] Y.K. Shin and J.H. Freed, Biophys. J. 55 (1989) 537; Y.K. Shin, D.E. Budil and J.H. Freed, Biophys. J. 65 (1993) 1283.
[5] P.G. de Gennes and C. Taupin, J. Phys. Chem. 86 (1982) 2294.
[6] J.I. Spielberg and E. Gelerinter, J. Chem. Phys. 77 (1982) 2159; Phys. Rev. B 30 (1984) 2319.
[7] E. Meirovitch, A. Nayeem and J.H. Freed, J. Phys. Chem. 88 (1984) 3454.
[8] G. Wikander, P.-O. Erikson, F.E. Burnell and G. Lindblom, J. Phys. Chem. 94 (1990) 5964.
[9] C. Chachaty, Can. J. Chem. 62 (1984) 1246.
[10] M. Ge and J.H. Freed, Biophys. J. 65 (1993) 2106.
[11] G.L. Millhauser, J. Gorcester and J.H. Freed, in: Electron magnetic resonance of the solid state, ed. J.A. Weil (Canadian Society for Chemistry, Ottawa, 1987).
[12] J. Gorcester, G.L. Millhauser and J.H. Freed, in: Advanced EPR: applications in biology and biochemistry, ed. A.J. Hoff (Elsevier, Amsterdam, 1989).
[13] J. Gorcester, G.L. Millhauser and J.H. Freed, in: Modern pulsed and continuous wave electron spin resonance, eds. L. Kevan and M.K. Bowman (Wiley, New York, 1990).
[14] G.L. Millhauser and J.H. Freed, J. Chem. Phys. 81 (1984) 37; 85 (1986) 63.
[15] L. Kar, G.L. Millhauser and J.H. Freed, J. Phys. Chem. 88 (1984) 3951.
[16] L. Schwartz, G.L. Millhauser and J.H. Freed, Chem. Phys. Letters 127 (1986) 60.
[17] J.P. Hornak and J.H. Freed, Chem. Phys. Letters 101 (1983) 115.
[18] S.A. Dzuba, A.G. Maryasov, K.M. Salikhov and Yu.D. Tsvetkov, J. Magn. Reson. 58 (1984) 95.
[19] G.G. Maresch, M. Weber, A.A. Dubinskii and H.W. Spiess, Chem. Phys. Letters 193 (1992) 134.
[20] J. Gorcester and J.H. Freed, J. Chem. Phys. 85 (1986) 5375; 88 (1988) 4678.
[21] J. Gorcester, S.B. Rananavare and J.H. Freed, J. Chem. Phys. 90 (1989) 5764.
[22] B.R. Patyal, R.H. Crepeau, D. Gamliel and J.H. Freed, Chem. Phys. Letters 175 (1990) 445, 453.
[23] J.H. Freed, G.V. Bruno and C.F. Polnaszek, J. Phys. Chem. 75 (1971) 3385.
[24] D.J. Schneider and J.H. Freed, Advan. Chem. Phys. 73 (1989) 387.
[25] D.J. Schneider and J.H. Freed, in: Spin labeling: theory and application, eds. L.J. Berliner and J. Reuben (Plenum Press, New York, 1989).
[26] S. Lee, B.R. Patyal and J.H. Freed, J. Chem. Phys. 98 (1993) 3665.
[27] D. Gamliel and J.H. Freed, J. Magn. Reson. 89 (1990) 60.
[28] S. Lee, D.E. Budil and J.H. Freed, to be published.
[29] L.J. Schwartz, Ph.D. Thesis, Cornell University (1984).
[30] R.R. Ernst, G. Bodenhausen and A. Wokaun, Principles of nuclear magnetic resonance in one and two dimensions (Oxford, New York, 1987).
[31] E. Meirovitch, D. Igner, E. Igner, G. Moro and J.H. Freed, J. Chem. Phys. 77 (1982) 3915.
[32] L.J. Schwartz, A.E. Stillman and J.H. Freed, J. Chem. Phys. 77 (1982) 5410.
[33] R.H. Crepeau, S. Saxena, S. Lee, B.R. Patyal and J.H. Freed, Biophys. J., in press.
[34] E. Rommel, F. Noack, P. Meier and G. Kothe, J. Phys. Chem. 92 (1988) 2981.